Universiteit
Leiden
The Netherlands

UV Photodesorption and photoconversion of interstellar ices: the laboratory perspective

Bulak, M.

Citation
Bulak, M. (2021, December 9). *UV Photodesorption and photoconversion of interstellar ices: the laboratory perspective*. Retrieved from https://hdl.handle.net/1887/3245781

Version:	Publisher's Version
License:	Licence agreement concerning inclusion of doctoral thesis in the Institutional Repository of the University of Leiden
Downloaded from:	https://hdl.handle.net/1887/3245781

Note: To cite this publication please use the final published version (if applicable).

4 | Photolysis of acetonitrile in a water-rich ice as a source of complex organic molecules: CH_3CN and H_2O:CH_3CN ices

Abstract

Many C-, O-, and H-containing complex organic molecules (COMs) have been observed in the interstellar medium (ISM) and their formation has been investigated in laboratory experiments. An increasing number of recent detections of large N-bearing COMs motivates our experimental investigation of their chemical origin. We investigate the potential role of acetonitrile (CH_3CN) as a parent molecule to N-bearing COMs, motivated by its omnipresence in the ISM and structural similarity to another well-known precursor species, CH_3OH. The aim of the present work is to characterize the chemical complexity that can result from vacuum UV photolysis of a pure CH_3CN ice and a more realistic mixture of H_2O:CH_3CN. The CH_3CN ice and H_2O:CH_3CN ice mixtures were UV irradiated at 20 K. Laser desorption post ionization time-of-flight mass spectrometry was used to detect the newly formed COMs *in-situ*. We examined the role of water in the chemistry of interstellar ices through an analysis of two different ratios of H_2O:CH_3CN (1:1 and 20:1). We find that CH_3CN is an excellent precursor to the formation of larger nitrogen-containing COMs, including CH_3CH_2CN, NCCN/CNCN, and $NCCH_2CH_2CN$. During the UV photolysis of H_2O:CH_3CN ice, the water derivatives play a key role in the formation of molecules with functional groups of: imines, amines, amides, large nitriles, carboxylic acids, and alcohols. We discuss possible formation pathways for molecules recently detected in the ISM.

Bulak, M., Paardekooper, D.M., Fedoseev, G., Linnartz, H., 2021, A&A 647, A82

4.1 Introduction

Astronomical detections of over 200 different molecules demonstrate the chemical diversity of the interstellar medium (ISM). Besides many smaller species, typically di- and triatomics, also a large amount of C-, O-, N- and H-bearing species has been identified that contain 6 or more atoms. From an astrochemical perspective these species are considered complex organic molecules (COMs) and make up 25 percent of the detected molecules (van Dishoeck 2014; McGuire 2018). Of special interest are 'prebiotic' species, a molecular subgroup that is relevant in the formation of amino acids or other molecules important for emergence of life. Nitriles are often considered as prebiotic molecules due to their ability to produce amides and carboxylic acids (including amino acids) upon hydrolysis in aqueous solutions. Acetonitrile (CH_3CN) is a part of this family as the simplest of the alkyl nitriles (Bernstein et al. 2002; Hudson et al. 2008).

CH_3CN is a symmetric top molecule with a large dipole moment of 3.92 D and in the gas phase it has been detected through its strong millimeter transitions. CH_3CN has been observed both in our Solar System and beyond (Cordiner et al. 2015; Goesmann et al. 2015; Woodney et al. 2002; Solomon et al. 1971; Bergner et al. 2018; Purcell et al. 2006; Calcutt et al. 2018). Whereas identifications so far are limited to the gas phase, it is generally assumed that CH_3CN is present on icy dust grains and plays an important role in solid state nitrogen chemistry (e.g. Loomis et al. 2013). Recently CH_3CN was identified towards the circumstellar disk around V883 Ori (Lee et al. 2019) where its origin as well as that of several other COMs - methanol, acetone, acetaldehyde and methyl formate - was directly linked to species sputtered from icy dust grains. These observations are in line with the idea that COMs form on icy dust grains through surface reactions that are triggered by impacting atoms, upon UV irradiation, electron bombardment, cosmic ray interactions or through thermal processing. In recent years many efforts have been taken to study such processes under fully controlled laboratory conditions. The results are then linked to astronomical observations or used as physical chemical input for astrochemical models. (e.g. Garrod & Herbst 2006; Garrod et al. 2008; Walsh et al. 2014b)

The majority of the identified COMs has been detected towards high-mass hot cores. Specific detections of nitriles and other nitrogen bearing species, including that of astrobiological importance, are: hydrogen cyanate (HCN), isocyanic acid (HNCO), formamide (NH_2CHO), methylamine (CH_3NH_2), methyl isocyanate (CH_3NCO), amino acetonitrile (NH_2CH_2CN), ethyl cyanide (CH_3CH_2CN), vinyl cyanide (CH_2CHCN), cyanoacetylene (HCCCN), acetamide (CH_3CONH_2), urea (NH_2CONH_2), (tentatively) N-methyl formamide (CH_3NHCHO), and more recently glycolonitrile ($HOCH_2CN$) and propargylimine (HCCCHNH) (Snyder & Bhul 1971; Bisschop et al. 2007b; Fourikis et al. 1974; Halfen et al. 2015; Ligterink et al. 2017; Belloche et al. 2009; Calcutt et al. 2018; Hollis et al. 2006; Belloche et al. 2019, 2017; Zeng et al. 2019; Bizzocchi et al. 2020).

In light of these detections and the prebiotic relevance of many nitriles, several studies have been focused on the involved formation pathways (Raunier et al. 2004; Jones et al. 2011; Danger et al. 2012). In comparison, many C-, O- and H-bearing COMs have been linked to UV irradiated CH_3OH ices (Öberg et al. 2009c; Paardekooper et al. 2016b). CH_3CN - even though less abundant in space - can be regarded as another promising parent molecule to yield its own branch of COM derivatives. Whereas the

formation of methanol through CO hydrogenation is well accepted (Watanabe et al. 2003; Fuchs et al. 2009; Linnartz et al. 2015), the interstellar formation pathways of CH_3CN are less known. In fact, both gas phase and solid state routes have been proposed. In the gas phase formation may proceed through radiative association:

$$HCN + CH_3^+ \rightarrow C_2H_4N^+ + \text{photon} \tag{4.1}$$

and followed by dissociative recombination:

$$C_2H_4N^+ + e^- \rightarrow CH_3CN + H \tag{4.2}$$

as proposed by Mackay 1999; Willacy et al. 1993; Vigren et al. 2008. In the solid state, formation of CH_3CN is possible through radical recombination, CH_3+CN (Garrod et al. 2008) or hydrogenation of C_2N (Belloche et al. 2009). Recent observational work by Loomis et al. 2018 indicates that the molecular origin of CH_3CN in the protoplanetary disk TW Hya is dominated by solid state pathways, in line with the already mentioned studies by Lee et al. (2019).

The first studies using CH_3CN as a solid state starting point in the formation of larger COMs were reported by Hudson & Moore 2004, Hudson et al. 2008 and Abdulgalil et al. 2013. Upon UV irradiation, the following photolysis products were identified: HCN, CH_4, and $(CH_2CN)_2$. It was also found that the parent species isomerizes to CH_3NC and H_2CCNH. When mixed with H_2O ice, photolysis of the CH_3CN:H_2O ice mixture yields OCN^-, one of the few charged ice species identified in space (van Broekhuizen et al. 2005) and characteristic of acid base chemistry forming a salt, $NH_4^+OCN^-$. Hudson et al. 2008 also showed that CH_3CN mixed with H_2O and bombarded with ions (at low temperature), resulted in the identification of amino acids after hydrolysis at room temperature. Danger et al. 2011 found that thermal processing of CH_3CN ice mixed with ammonia resulted in the formation of amino acetonitrile. Hydrolysis of amino acetonitrile in liquid solution at room temperature is known to form glycine.

Whereas UV photolysis of CH_3CN ice clearly showed to trigger solid state chemical processes, hydrogenation of CH_3CN by thermalised H atoms was found to be rather inefficient due to a high energy barrier for the first H atom addition (Nguyen et al. 2019). Conversely, for the hydrogenation of isonitrile CH_3NC the barrier was found to be lower and lead to the formation of secondary amines (CH_3NHCH_3). Other chemical routes may also be relevant in the formation of N-bearing prebiotics. Gerakines et al. 2004 studied the photolysis and proton irradiation of H_2O:HCN mixture, which yielded isocyanic acid (HNCO), formamide (NH_2CHO), OCN^- and NH_4^+, and recently Ligterink et al. 2018a demonstrated solid state pathways to form amides upon UV irradiation of an CH_4:HNCO ice mixture.

In the present work the focus is on UV induced reactions in pure CH_3CN ice and H_2O:CH_3CN ice mixtures. The aim is to demonstrate the formation of heavier COMs. This becomes possible through application of a new ultra-sensitive detection method based on laser desorption post ionization time-of-flight mass spectrometry, with experimental details described in section 4.2. The primary goal is to improve our understanding of solid state astrochemical reactions that extend existing networks resulting in the formation of (N-bearing) COMs. The results are presented and discussed in section 4.3. Information on the underlying reaction network showing how imines, amines, amides and nitriles chemically connect and the "catalytic" role of water are presented. The manuscript concludes with the astronomical relevance of this work.

4.2 Experimental

The experiments are performed in an ultra-high vacuum (UHV) system, MATRI^{2}CES (Mass Analysis Tool to study Reactions in Interstellar ICES). This section provides the relevant information, while a detailed description of MATRI^{2}CES can be found in Paardekooper et al. 2014. The experimental procedures as well as an overview of the experiments performed are discussed.

4.2.1 Setup and analysis tools

MATRI^{2}CES is a two chamber system, with a base pressure in the 10^{-10} mbar range. The main chamber houses a closed cycle Helium cryostat which cools a 2.5 cm x 5 cm large gold coated copper substrate to a temperature of 20 K. A thermocouple and a resistive heater are attached to the cold finger, allowing a Lakeshore 331 temperature controller to regulate the temperature of the substrate between 20 and 300 K with roughly 1 K precision. Ice growth on the substrate proceeds via needle valves that guarantee a continuous and stable deposition pressure in the main chamber. The needle valve on the front is connected to a tube which faces the sample at an angle of 85 degrees with respect to the substrate. Acetonitrile (CH_3CN, VWR, <10ppm of water), and acetonitrile-D3 (CD_3CN, Sigma-Aldrich, $\geq$ 99.8% D) are used. In order to simultaneously admit water vapor (H_2O, miliQ or $H_2{}^{18}O$, Sigma-Aldrich, 97% ^{18}O), an additional needle valve located behind the substrate is used. Prior to deposition, atmospheric gases trapped in the samples are removed by several freeze-pump-thaw cycles. The growth rates are determined in advance by HeNe interference measurements as discussed in previous works (Baratta & Palumbo 1998; Paardekooper et al. 2016c; Bulak et al. 2020).

UV irradiation of the ice is accomplished with a microwave discharge hydrogen flowing lamp (MDHL, F-type), which is connected to the main chamber by a magnesium fluoride (MgF_2) viewport and directly faces the substrate. The lamp produces vacuum UV photons with energies in the 7-10.2 eV range and simulates interstellar radiation fields. Throughout all experiments, the lamp is run at a H_2 pressure of 1.4 mbar and 80 W of microwave power. The corresponding SED contains both Lyman-α (121.6 nm) and molecular H_2 emission continuum (130 - 165 nm); the full SED is given in Fig. 4 in Paardekooper et al. 2016c. The impacting radiation causes various processes in the ice molecules, e.g., excitation, dissociation, desorption or even ionisation in the case if ionization threshold is below the energy of the present UV photons. For an overview of photo-induced processes see Fig 1 in Bulak et al. 2020. The photon flux of the MDHL is measured at the location of the substrate with a NIST calibrated photodiode and found to be $(2.5 \pm 0.5) \times 10^{14}$ photons cm^{-2}s^{-1}.

As analytical technique, laser desorption post ionisation time-of-flight mass spectrometry (LDPI TOF-MS) is applied to probe the composition of the ice at different vacuum UV fluences. The light of an unfocused ($\sim$1 mm) Nd:YAG laser beam (355 nm and 4-5 ns pulse length) is used as an ice ablation source. Typical laser pulse energies of 65 mJ cm^{-2} are applied. Ice species that are desorbed are subsequently ionized in the gas phase using 70 eV electrons and guided by ion optics located in front of the substrate into the second chamber, which contains a field free TOF system. The latter is operated in reflectron mode to increase mass resolution (Δm/m $\sim$250). In order to select different parts of the photoprocessed ice for sequential laser ablation

steps, the position of the cryostat (and substrate) can be moved using a two dimensional translation stage. In the vertical direction, translation is driven by a stepper motor, and in the horizontal direction, it is manually controlled. The motorized vertical translational stage allows for synchronization with laser shots resulting in each shot probing a fresh location on the ice, while ensuring that the location of the desorption plume with respect to the ion optics remains the same. This approach results in minimal shot-to-shot fluctuations, while ensuring that multiple averages can be used to increase the overall signal-to-noise. Every mass spectrum presented in this study is based on 100 averages obtained at different locations on the ice coated substrate. To trace the changes in the chemical composition of the ice, raw TOF spectra are collected at different photon fluences. In order to determine the elemental compositions of the new signals in the mass spectra, each experiment is performed for two isotopes. For the pure ice, CH_3CN and CD_3CN, and for the mixed ices, CH_3CN:$H_2{}^{16}O$ and CH_3CN:$H_2{}^{18}O$ are used.

The dominating process driving the reactions in the ice is photodissociation followed by radical-radical and radical-molecule interactions. Hence, the combination of elemental composition of the new ions, with fragmentation patterns of the expected products from the NIST database, allows to tentatively identify the newly formed photoproducts. In addition, based on the order of appearance of the new mass peaks, assigned species can be roughly separated into first and second generation photoproducts.

Quantitatively, the mass spectra are analysed by calculating the integrated area of each peak by fitting a Pearson IV distribution (Castellanos et al. 2018). This function allows for peak asymmetry and therefore is able to accurately fit the individual peaks. The resulting intensities of mass peaks can be regarded as a linear combination of multiple individual compounds present in the plume (Paardekooper et al. 2014). Hence, an integrated mass spectrum, M_t, at a given irradiation time, t, can be expressed by:

$$M_t = \sum_{i=1}^{n} a_i \cdot \sigma_i \cdot M_i, \tag{4.3}$$

where a_i is the molecular abundance of species i, σ_i is the ionization cross section and M_i is the corresponding fragmentation pattern. To derive product abundances, we fit our experimental data using a limited memory Broyden–Fletcher–Goldfarb–Shanno (L-BFGS) optimisation algorithm incorporated in Python. This allows to take into account all parameters from equation 4.3 and trace the evolution of different species in the ice throughout the VUV photo-processing. Where available, NIST mass spectra are used as input for the reference mass spectra.

4.2.2 Overview experiments

Table 4.1 summarizes all relevant experiments. The experiments allow to get an insight into the early stages of the photolysis process. At a low photon fluence, the radical concentration in the ice is low, hence, the impact of the second order reactivity, including reversed reactions, is limited. The experiments are extended to be representative for a lifetime of a dense molecular cloud, which may experience a total fluence as high as (3-30) $\times$ 10^{17} photons cm^{-2}. This value has been estimated using a cosmic ray induced UV flux of (1-10) $\times$ 10^3 photons $cm^{-2}s^{-1}$ and an average molecular cloud life-

Table 4.1: Summary of the performed CH_3CN and H_2O:CH_3CN UV photolysis experiments. The UV irradiation time is given in minutes, with a photon flux of $(1.5 \pm 0.5) \times 10^{15}$ photons $cm^{-2}min^{-1}$.

Composition	Thickness (ML)	Temperature (K)	UV irradiation (min)
CH_3CN*	40	20	0-128
CH_3CN	40	77	0-128
CH_3CN	40	20-285	0-128
CD_3CN*	40	20	0-128
H_2O:CH_3CN* (∼1:1)	100	20	0-128
H_2O:CH_3CN* (∼20:1)	100	20	0-128
$H_2{}^{18}O$:CH_3CN* (∼20:1)	100	20	0-128
blank*	0	20, 160-300	60

Notes. Experiments repeated more than once are marked with an asterisk (*)

time of up to 10^7 years (Shen et al. 2004a). The CH_3CN and complimentary CD_3CN experiments are conducted to confirm product assignments. The same approach is used for two different H_2O:CH_3CN ice mixtures. Most experiments are performed at a temperature of 20 K, however, in order to apply the results to different environments, such as the icy surfaces of Titan, data is also collected at 77 K.

To provide an additional tool for identification of photoproducts according to their characteristic desorption temperatures (Paardekooper et al. 2016c), an experiment with a range of temperatures (20-285 K) is performed for CH_3CN. In this experiment, the ice is UV-irradiated at 20 K, then slowly warmed up and probed with LDPI. For example, the mass peaks representing methane, at a temperature above its thermal desorption (∼40 K), decrease in signal, confirming the assignment of methane.

The blank experiment is performed to demonstrate that all detected reaction products form in the deposited ice, rather than externally, i.e., on the walls of the setup or in the ion optics. To test that, the cold substrate (20 K) is UV irradiated and probed via LDPI. This procedure is also performed at higher temperatures, following a deposition of CH_3CN above its thermal desorption threshold (160-300 K). In all experiments, the dominant uncertainty source follows the absolute calibration of the deposition rate and UV flux. The error bars shown in the kinetics diagrams are a result of the fitting routine of the particular mass peaks.

4.3 Results and discussion

This section comprises of three parts. First the photolysis of pure CH_3CN ice is discussed. The LDPI TOF-MS data are presented and photoproducts are assigned. The production yields of first generation photoproducts are calculated. Second, a similar qualitative analysis is done for the UV photolysis of H_2O:CH_3CN ice mixtures. The photoproduct assignments are additionally supported by mass spectra from experiments for two different mixing ratios (1:1 and 20:1). In the third part the chemical

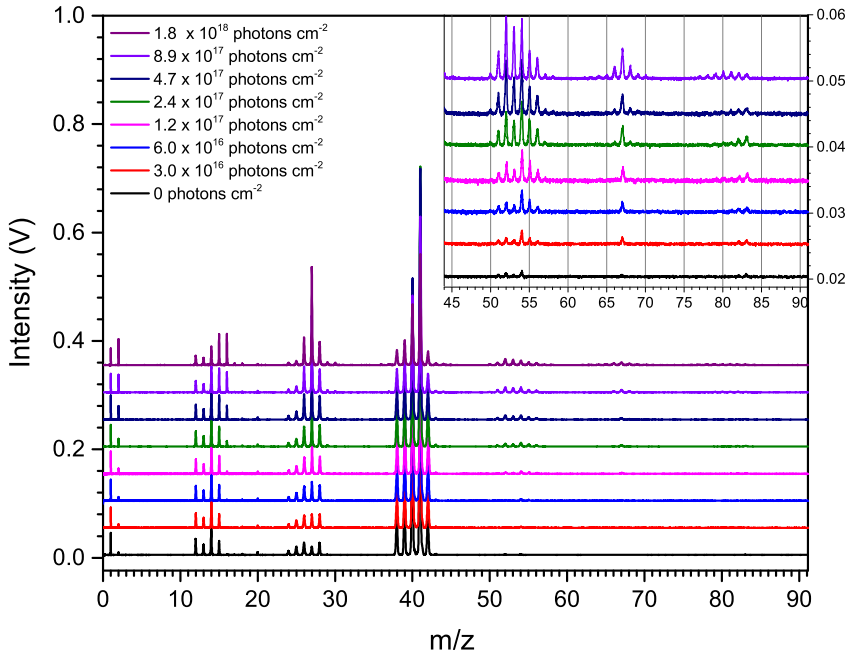

Figure 4.1: LDPI-MS signals for an UV irradiated CH_3CN ice at 20 K for increasing photon fluence. The lowest graph shows the signal without UV irradiation. The inset is a zoom in on the intensity scale for the higher masses.

role of water molecules is presented.

4.3.1 CH_3CN photoproducts

Mass spectra obtained throughout the UV photolysis of pure CH_3CN ice are shown in Figure 6.1 The bottom trace shows the signature of an unprocessed acetonitrile ice with a characteristic fragmentation pattern spread over multiple mass peaks (m/z = 12-15, 24-28, 38-42). It serves as a reference for tracking any changes in the chemical composition of the ice. After 2 min of UV irradiation (3.0×10^{16} photons cm^{-2}, represented by the red trace), new peaks arise at m/z values: 16, 27-29, 51-56, 67, 82, 83. As photolysis proceeds (see the remaining traces) additional peaks appear in the spectra, demonstrating a rapid increase in the total number of species newly formed in the ice. The (inset in the) figure also shows the high detection sensitivity of MATRI^{2}CES and its capability to quickly monitor the formation of larger COMs, up to at least 6-7 C/N-atoms containing species (m/z = 93).

The assignment of the new peaks to specific molecules is not straight forward as the peaks merely reflect fragment masses due to the dissociative ionization method (electron impact ionization): upon dissociation different species may form identical fragments. Also, it is not *a priori* clear which species are expected to form as different

processes are involved. Radicals created via photodissociation recombine with each other to form larger stable products. The MDHL produces photons in the energy range between 7-10.2 eV, which is below the ionization potential of the CH_3CN, but is sufficient to overcome a barrier for two photodissociation pathways: CH_2CN-H and CH_3-CN with thresholds of 4 and 5.2 eV, respectively (Darwent 1970). Moreover, the formed CN radicals can be in electronically excited states (Kanda et al. 1999; Schwell et al. 2008). Given their high reactivity, the radicals do not build up an abundance sufficient to be detected directly. Instead, the stable end products of radical recombination can be studied. The radicals can also react with the abundantly present precursor species (CH_3CN), e.g. by interacting with the triple CN bond. Alternatively, it is possible that newly formed species (e.g. CH_3CH_2CN) can engage in a neutral-radical reactions or be photodissociated to supply a new, large radical for further reactions, as discussed in detail by Fedoseev et al. 2017. It is also possible that the resulting radicals participate in H-atom abstraction reactions (Chuang et al. 2016).

An assignment of the mass peaks shown in Fig. 6.1 to specific species starts with the determination of the elemental composition of the new mass peaks. The observed mass peaks reflect either the ionized (and unfragmented) species formed along one of the three processes described above, or one of the corresponding photoproduct fragments formed upon dissociative ionization. In addition, CD_3CN is used as an isotopically enriched precursor to discriminate between mass peaks shifted because of hydrogen and deuterium contributions. Special care is taken that the overlap between the chosen characteristic peaks is minimum. In this way it is possible to link the majority of the observed mass peaks to an elemental C/N/H composition and this allows to conclude on the formation of several of the formed products, as will be illustrated later. Table 4.2 gives a summary of the observed mass peaks used to derive the elemental product composition and (tentative) assignments of species, newly formed upon VUV photolysis of pure acetonitrile ice.

In Table 4.2 photoproducts formed as a result of isomerization are included, but their identification (and presence in the ice) cannot be confirmed using tof mass spectrometry. Here, tandem mass spectrometry or spectroscopic methods would offer a possible alternative. This applies to most nitriles being restructured into isonitriles (e.g. $CH_3CN \rightarrow CH_3NC$) and acetonitrile isomerizing into ketenimine ($CH_3CN \rightarrow H_2C{=}C{=}NH$), which has been discussed by Hudson & Moore 2004.

To demonstrate the approach to photoproduct assignments, Figure 6.2 highlights the isotopic shift between the CH_3CN and CD_3CN experiments. Upon VUV irradiation, an immediate increase in signals at m/z = 16 and 27 is observed for CH_3CN (red trace), which corresponds to an increase at m/z = 20 and m/z = 28 when using the deuterated equivalent. The corresponding elemental compositions are CH_4 and HCN which are obviously assigned to methane and hydrogen cyanide. Possible formation pathways of these species include hydrogenation of the CN and CH_3 radicals, as demonstrated in previous studies (Borget et al. 2017; Qasim et al. 2020). For higher UV fluences (blue and pink traces), the abundance of these products continues to increase, while other peaks demonstrate further changes in the composition of the ice. Towards the end of CH_3CN photolysis, peaks at m/z = 26, 28, 29 and 30 increase.

Table 4.2: Characteristic m/z peaks used for identification of photoproducts of the UV photolysis of the CH_3CN ice

CH_3CN m/z	CD_3CN m/z	Elemental composition	Proposed molecular species	Name
2	4	H_2	H_2	mol. hydrogen
16	20	CH_4	CH_4	methane
26, 27	26, 28	CNH	HCN/HNC	hydrogen (iso)cyanide
40, 41	42, 44	C_2NH_3	$CH_3CN/CH_3NC/H_2CCNH$	acetonitrile/methyl isocyanide/ketenimine
50, 51	50, 52	C_3NH	HCCCN	propiolonitrile
52	52	C_2N_2	$(CN)_2$	cyanogen
26, 52, 53	26, 54, 56	C_3NH_3	CH_2CHCN	2-propenenitrile
28, 54	30, 58	C_3NH_5	CH_3CH_2CN	propanenitrile
29, 55	32, 60	C_3NH_5	CH_3CH_2NC	ethyl isocyanide
56	62	C_3NH_6	-	imine (R-CHNH)
65-69	66, 68, 70, 72, 74	$C_3N_2H_x$	-	
77-83	78-90	$C_4N_2H_y$	-	-

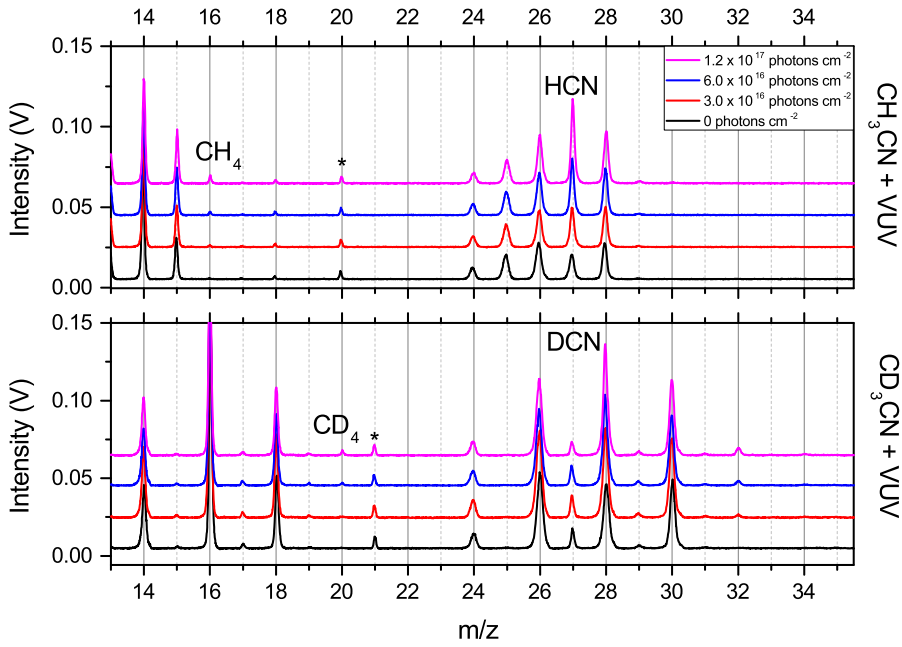

Figure 4.2: Low m/z range of LDPI-MS signals of pure CH_3CN (top panel) and CD_3CN (bottom panel) at 20 K, as a function of photon fluence. Peak marked by an asterisk (*) is a doubly ionized CH_2CN^{2+}.

This mass range is characteristic for fragments of large (iso)nitrile species (CH_3CH_2CN, CH_2CHCN and CH_3CH_2NC). However, small species, if present in the ice (methanimine CH_2NH), might also contribute. Following the outcome of the deuterated experiments, these peaks can be matched with the following elemental compositions: CN/C_2H_2, CNH_2/C_2H_4, CNH_3 and CNH_4.

The higher m/z range is analyzed using the same strategy, as shown in Figure 6.3. Newly observed peaks are assigned to elemental compositions of C_2N_2, C_3NH_x, $C_3N_2H_x$ and $C_4N_2H_y$ (x = 1, 3, 5 and y = 1, 3, 5, 7). The mass peak at m/z = 52, which is clearly visible in both experiments, is assigned to (iso)cyanogen (NCCN/CNCN). Based on characteristic mass peaks of (iso)nitriles with three carbon atoms (NIST Chemistry Webbook), the signals at 50-55 amu are assigned to a combination of propiolonitrile (HCCCN), acrylonitrile (CH_2CHCN), propanenitrile (CH_3CH_2CN), and ethyl isocyanide (CH_3CH_2NC). The formation of NCCN/CNCN and CH_3CH_2CN probably proceeds via radical recombination reactions. Peaks representing CH_2CHCN and HCCCN appear later in the photolysis, which can be interpreted as a result of UV-induced dehydrogenation of CH_3CH_2CN.

The peak at m/z = 56 shifts to m/z = 62 in the deuterated experiments. This observation is consistent with C_3NH_6 elematal composition which can only be obtained by hydrogenation of CN bond bond. This leads to imine formation, with a general structure of R-CHNH. As the involved fragmentation pattern is not known, it is unfortunately not possible to unambiguously confirm this assignment.

Mass peaks in the range of m/z = 65-69 and m/z = 77-83 have been assigned with

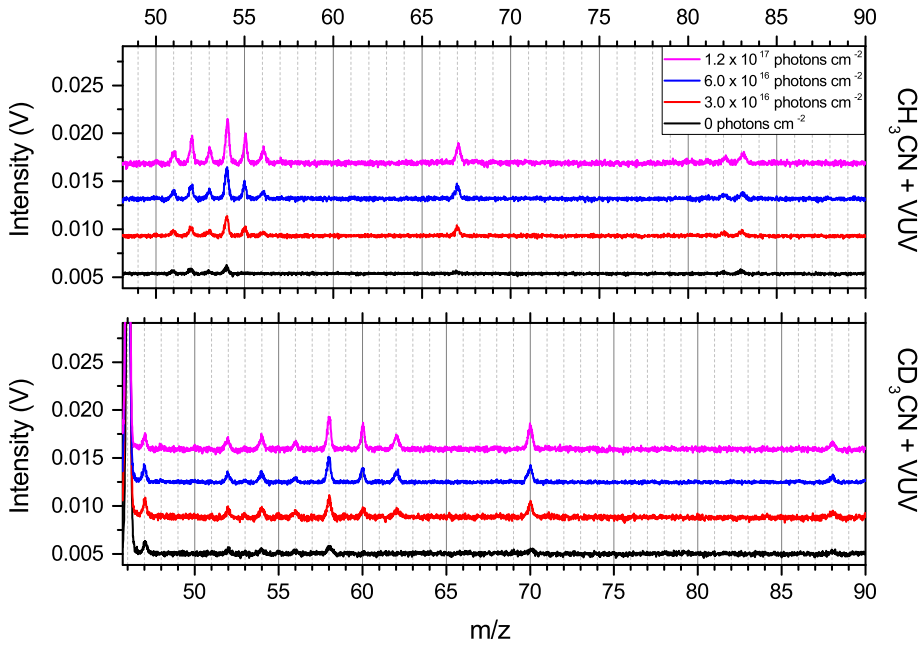

Figure 4.3: High m/z range of LDPI-MS signals of pure CH_3CN (top panel) and CD_3CN (bottom panel) at 20 K, as a function of photon fluence.

elemental compositions $C_3N_2H_x$ (x = 1, 3, 5) and $C_4N_2H_y$ (y = 1, 3, 5, 7). Due to the visibility of traces at m/z = 67, 82 and 83 in the reference spectrum (before photolysis), and a significant increase of these signals during the experiments, it is likely that these represent newly formed large photolysis products. For this it is important to exclude that these peaks are a direct consequence of the used laser desorption method or originate from non-volatile residues from previous experiments.

It has been demonstrated that upon laser desorption, species with strong hydrogen bonds, such as H_2O, CH_3OH or CH_3CN, form protonated clusters (e.g. $(H_2O)_nH^+$, where n = 0, 1, 2 and higher from Gudipati & Yang 2012). Mass peaks of these clusters are easily recognized, as the corresponding peaks are evenly spaced and their intensities decrease with the size of the cluster (n). Additionally, the intensity of the cluster peaks follows the abundance of the parent molecule. Hence, if CH_3CN abundance decreases, any peaks assigned to $(CH_3CN)_nH^+$ (where n = 0, 1, 2) should follow this trend (Ribeiro et al. 2020). This behaviour is not seen in our spectra (see Figure 6.1). On the contrary, the peaks at m/z = 65-69 and m/z = 77-83 increase, while the parent species decreases, hence these peaks do not originate from clustering upon laser desorption. Blank experiments are performed, to exclude the role of any non-volatile residue on the substrate left over from previous experiments. At an increased laser power (doubled) and detector voltage (increased by 300 V), some residue is detected. Subsequently, the substrate is irradiated for 1 hr and new small mass peaks are observed in the mass spectra. Special care is taken to tune the experimental settings (laser power and MCP detector voltage) to minimize observations of any resid-

ual material. Consequently, at the standard sensitivity settings (Section 4.2), neither the residue, nor its derivatives, are observed. This leaves the conclusion that the new signals represent newly formed photoproducts arising from CH_3CN photolysis.

After 2 min of UV photolysis, the mass peak at m/z = 67 dominates the higher region of the mass spectrum. The elemental composition of this ion corresponds to a combination of CH_3CN and a CN radical, however, to our knowledge, there are no stable molecules of that composition. This implies that it likely is a fragment of a larger molecule. The simplest scenario is that the fragment at m/z = 67 is the main fragmentation channel (molecular ion minus H) of a molecule with an elemental composition of $C_3N_2H_4$. An intense H-loss channel upon electron ionization, is typical for nitriles. The only stable candidate found in the NIST database that matches this elemental composition is glycinonitrile, n-methylene- $NCCH_2NCH_2$. Unfortunately, due to a lacking fragmentation pattern, it is not possible to confirm this assignment. At longer irradiation times, additional peaks appear near m/z = 67, suggesting subsequent (de)hydrogenation reactions (+2H or -2H). Similarly to m/z = 67, it is not possible to unambiguously assign molecular formulas to these ions.

Due to lack of available fragmentation patterns of large nitriles, the identification of ions at m/z = 77-83, in most cases, follows the assignment of the elemental composition. An exception is succinonitrile ($NCCH_2CH_2CN$), suggested to be a photolysis product in previous studies (Hudson et al. 2008). The fragmentation pattern of $NCCH_2CH_2CN$, with strong peaks at m/z = 79, and 80 fits the experimental spectrum. The assignment is supported via an available formation pathway: a recombination of two CH_2CN radicals, which at a high UV fluence, are abundant in the ice. Peaks which are near succinonitrile features differ in the number or hydrogen atoms, but that can be accounted for by +2H and -2H reactions, resulting in formation of unsaturated nitriles, and imines, respectively.

VUV irradiation of CH_3CN ice at a higher temperature of 77 K shows the same molecular complexity in the ice, with one exception. That is a lower production yield of methane. This can be explained by methane thermally desorbing from the ice, as its desorption temperature (40 K) is below the photolysis temperature of 77 K. We conclude that the ice photochemistry of CH_3CN results in a similar complexity in the temperature range between 20 and 80 K. It also implies that thermally initiated reactions do not play a (major) role in this temperature range.

As mass spectra are recorded for different fluences, it is possible to visualize the formation kinetics for the main CH_3CN photoproducts (20 K), listed in Table 4.2. The absolute ice abundances are shown in Figure 6.4, calibrated using the known initial abundance of the parent molecule. For this, complete fragmentation patterns of products described above were fitted to our data. This was followed by considering the electron impact ionization cross sections of the species which were taken from the NIST database (Kim et al. 2014) or theoretical work (Pandya et al. 2012; Zhou et al. 2019).

The HCN abundance exhibits the fastest increase and appears to be the most abundant product during photolysis. Simultaneously, at a 10 times lower formation rate, CH_3CH_2CN and CH_4 are formed in the ice. A potential origin of the significant difference in formation yields is discussed in section 4.3.3. As the photon fluence increases, methane becomes the second most abundant product. The remaining quantified products are: NCCN/CNCN, and CH_2CHCN, at significantly lower abundances, compared to HCN. The formation of H_2 is also observed, however, its yield is largely

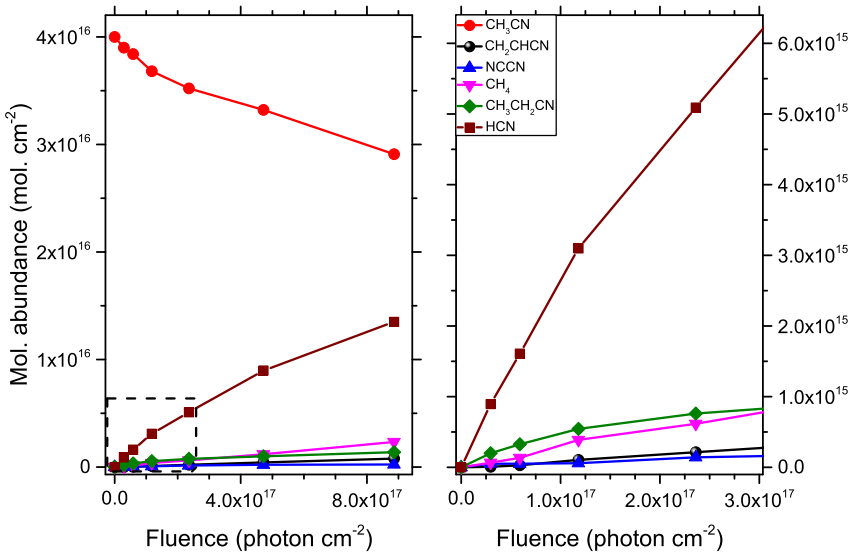

Figure 4.4: *Left panel:* Molecular abundances of species during the UV photolysis of CH_3CN ice as function of photon fluence. *Right panel:* Zoom in of the low fluence region indicated in the left panel.

limited by its thermal desorption. The molecular yields of all quantified photoproducts are summed up to check if the formation of new species balances the loss of the parent molecules. That is indeed the case, hence, despite unidentified peaks appearing in the ice, their contributions to the early chemical network are considered insignificant. The formation kinetics for photoproducts of CD_3CN at 20 K (not shown here) demonstrate similar trends.

4.3.2 H_2O:CH_3CN

Two different H_2O:CH_3CN ice mixing ratios are used (1:1 and 20:1). Figure 6.5 shows the calibrated LDPI TOF-MS data of the photolysed water rich (20:1) mixture for selected VUV fluences. The (black) reference spectrum, before irradiation, shows m/z peaks which can be assigned to fragmentation patterns of H_2O (m/z = 16-18), CH_3CN (m/z = 12-15, 24-28, 38-42) and protonated clusters of water and water-acetonitrile (m/z = 19, 37, 55, 60, 73). The latter are not formed upon VUV irradiation but are known to form upon laser desorption. After 2 minutes of irradiation, an increase in the following mass signals is observed: 27-34, 42-46, 51-60, 75, 76, 93, 94 (see inset of Fig. 6.5). As the photolysis continues, more peaks are formed. By comparing Figures 6.1 and 6.5 it is immediately clear that the level of molecular complexity is higher in the water containing ice. This is also expected. Upon UV irradiation, the ice contains OH radicals, as well as O- and H-atoms that will expand the chemical network. A systematic analysis of the resulting data is given below.

A comparison of the pure and mixed ice (1:1) allows to identify mass peaks that

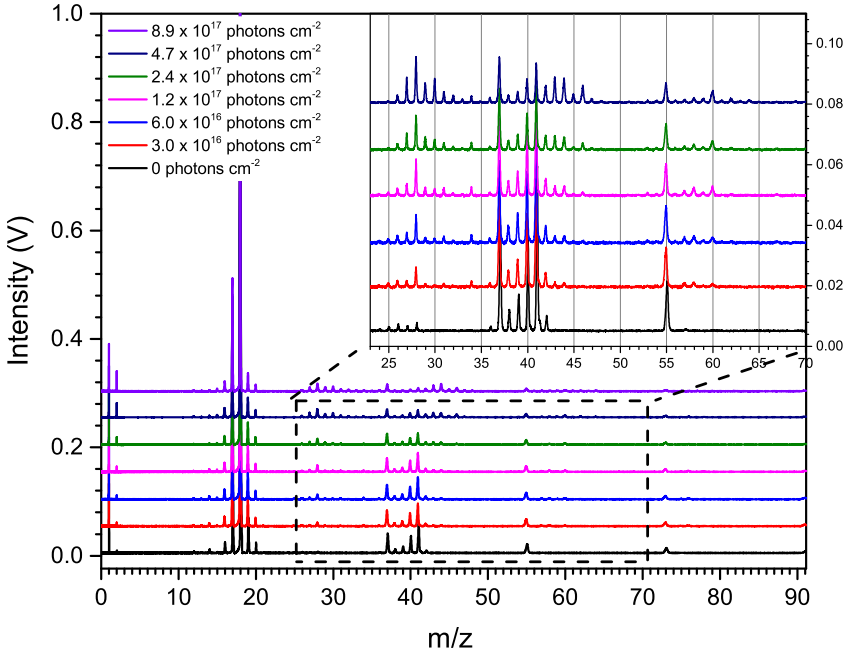

Figure 4.5: LDPI-MS signals for an UV irradiated H_2O:CH_3CN (20:1) ice at 20 K for increasing photon fluence. The lowest graph shows the signal without UV irradiation. The inset is a zoom in on the intensity scale for the higher masses.

can be associated with water chemistry. In the water dominated experiments (20:1) the abundance of these products is expected to further increase. This information, combined with TOF spectra obtained for the $H_2{}^{18}O$ experiments, allows to assign the elemental compositions of the produced species. Finally, considering the reactions expected to take place in the ice mixture, specific mass peaks can be linked to specific (fragments of) photoproducts, similar to the approach used for pure ices. Table 3.3 shows a summary of all observed mass peaks and their corresponding elemental compositions.

The results of four different photolysis experiments: pure CH_3CN ice, two different H_2O:CH_3CN mixtures (1:1 and 20:1) and a $H_2{}^{18}O$:CH_3CN mixture (20:1), are shown in Figures 4.6, 4.7 and 4.8. Each figure shows a different mass range; it is noted that Fig. 4.6 shows the intermediate range (37-50 amu) and Figs 4.7 and 4.8 a lower (24-37 amu) and higher (50-70 amu) mass regime, respectively. In order to compare relative yields of products between the four experiments, all mass spectra are normalized to the amount of CH_3CN in the ice via the mass peak signal at m/z = 39. This particular peak is chosen as a signature of acetonitrile, as it does not with overlap with any other fragments of species present in the ice.

Figure 4.6 shows a mass spectral range between m/z = 37-50. Peaks at 38-42 amu are a part of the fragmentation pattern of CH_3CN ice. The VUV irradiation of the (1:1) ice mixture yields new mass peaks at m/z = 45-48 and signals at m/z = 42, 43,

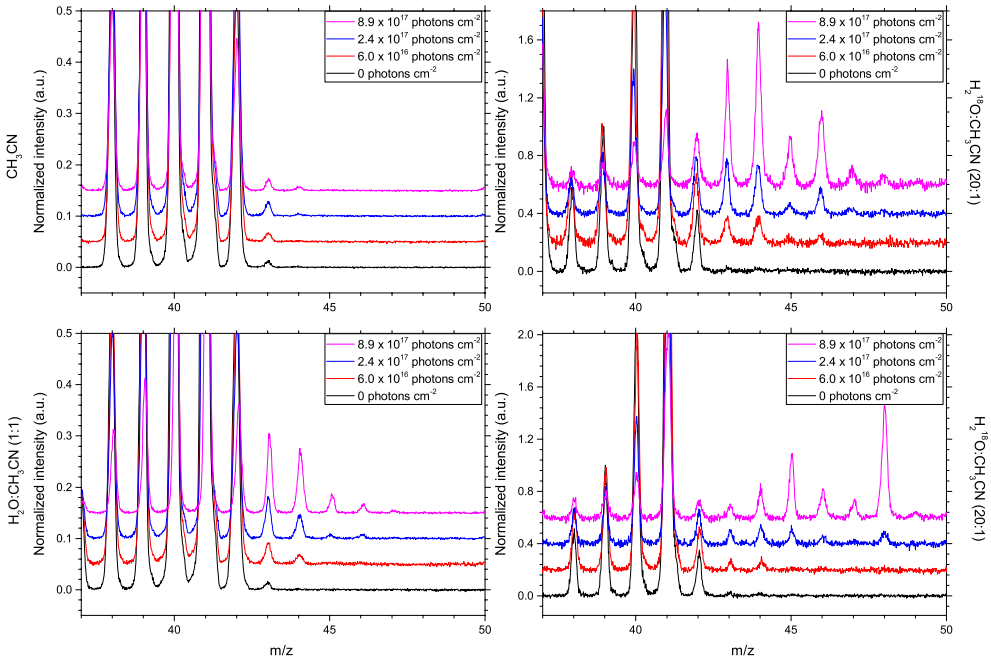

Figure 4.6: Normalized LDPI-MS signals (m/z range: 37-50) for four different photolysis experiments. Top panel from left to right: CH_3CN, H_2O:CH_3CN (20:1). Bottom panel from left to right: H_2O:CH_3CN (1:1) and CH_3CN:$H_2{}^{18}O$ (20:1).

44 are significantly higher than in the pure ice experiment. The new peaks hint at the presence of O-bearing species, which is consistent with the TOF spectra found for the water dominated experiment (20:1). A comparison of the (20:1) spectra for the ^{16}O and ^{18}O water shows that not all product peaks (42-48 amu) can be assigned to O-bearing species, as only part of the peaks shifts upon ^{18}O substitution.

The observed peak shifts, corresponding to 2 or 4 amu, indicate that O-bearing species/fragments are involved with one or two oxygen atoms. The corresponding elemental compositions are: CHNO, CH_3NO, CO_2H_{2x} and C_2H_yO (where x = 0, 2 and y = 4, 6). Based on the characteristic mass peaks of all considered species, these compositions can be assigned to isocyanic acid (HNCO), carbon dioxide (CO_2), acetaldehyde (CH_3CHO), dimethyl ether (CH_3OCH_3), ethanol (CH_3CH_2OH) and formic acid (HCOOH). Formamide (NH_2CHO) is one of the candidates fitting the CH_3NO composition, and several possible solid state formation routes have been discussed before (Raunier et al. 2004; Jones et al. 2011; Ligterink et al. 2018a), but other isomers cannot be excluded at this stage. The assignment of the elemental formula HCNO to isocyanic acid is guided by a previous study (Gerakines et al. 2004) and the greater stability of HNCO versus its isomers by Crowley & Sodeau 1989.

The contribution from other species in the m/z = 42-48 range is only clearly visible in the ^{18}O experiments. All oxygen containing species shift to m/z = 45 or higher, while peaks at 42, 43, and 44 remain present in the spectra. Molecules which contribute to these peaks lack oxygen. Considering the parent species, it was concluded that these mass signals originate from imines (containing the = NH functional group)

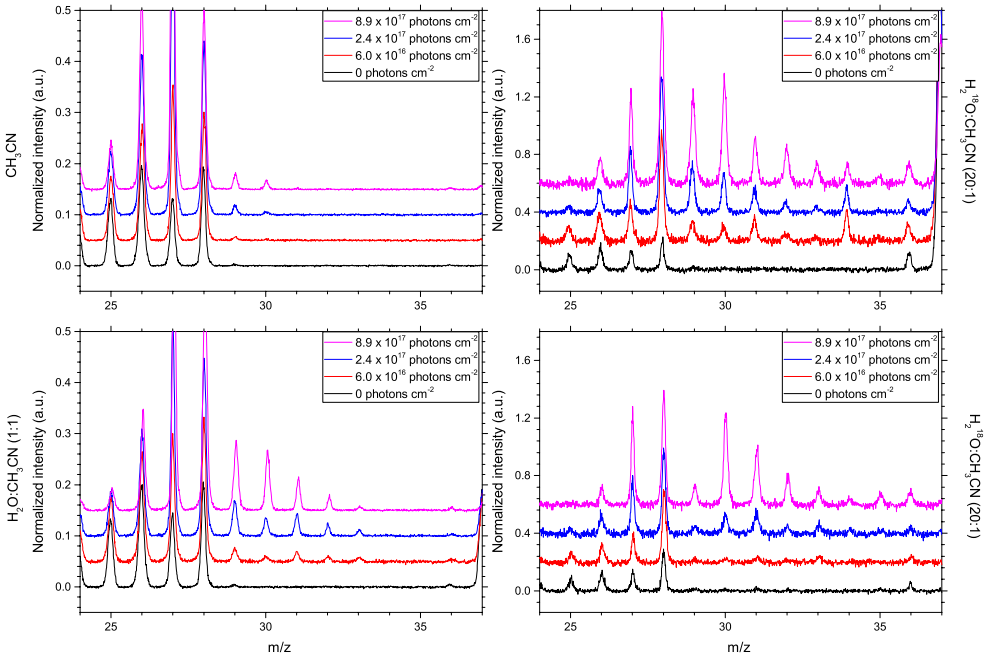

Figure 4.7: Normalized LDPI-MS signals(m/z range: 24-37) for four different photolysis experiments. Top panel from left to right: CH_3CN, H_2O:CH_3CN (20:1). Bottom panel from left to right: H_2O:CH_3CN (1:1) and CH_3CN:$H_2{}^{18}O$ (20:1).

and amines (containing the -NH_2 group). It is important to note that as the signals in the ^{18}O experiments are generally less intense, partially due to the presence of 3% of ^{16}O, this does not account for the observed signals at m/z = 42-44. A similar process was demonstrated for HCN, which undergoes hydrogenation reactions, even with cold atoms, to form CH_2NH_2 (Theule et al. 2011).

The present work demonstrates, for the first time, the hydrogenation of a CN bond for larger nitriles. The formation of imines and amines seems to be significantly enhanced in the presence of water ice. This has two major consequences. Firstly, it underlines the "catalytic" potential of water ice. Secondly, it implies that =NH and $-NH_2$ functional groups are present in the ice, which helps with interpreting the mass signals in the other mass ranges. The addition of water into the ice mixture clearly increases the number of possible chemical pathways and is further discussed in Section 4.3.4.

Figure 4.7 shows a lower mass range (m/z = 24-37) which is the signature region of smaller COMs. A comparison of the UV irradiated pure and mixed ices (1:1), shows that new mass signals appear at m/z = 31, 32, 33, while at m/z = 29 and 30 significantly higher signals are found. The peak at m/z = 32, which further increases with water content (20:1) is determined to have an elemental composition of CH_4O. With CH_3 and OH radicals available in the ice, the most logical explanation is that this peak corresponds to the ionized methanol (CH_3OH^+). This assignment is consistent with the shift of the peak (m/z = 32 to m/z = 34) in the ^{18}O experiments and with the increasing intensity of the methanol base peak (m/z = 31, shifted to m/z = 33),

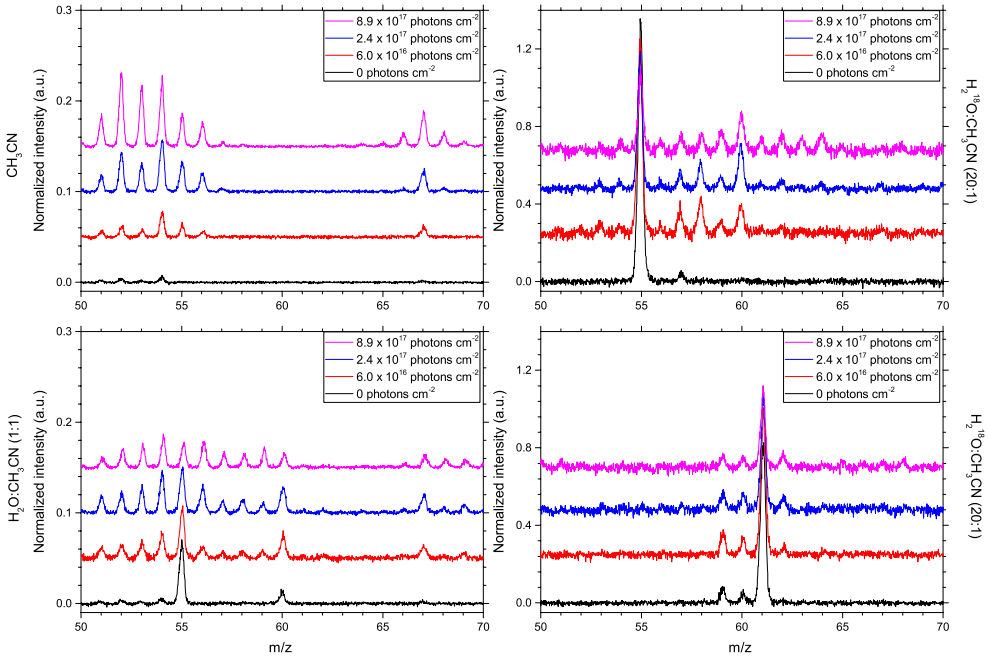

Figure 4.8: Normalized LDPI-MS signals (m/z range: 50-70) for four different photolysis experiments. Top panel from left to right: CH_3CN, H_2O:CH_3CN (20:1). Bottom panel from left to right: H_2O:CH_3CN (1:1) and CH_3CN:$H_2{}^{18}O$ (20:1).

although it should be noted that this peak is also characteristic for fragment masses of larger COMs. The formation of methanol also indicates that CH_3OH photoproducts as studied by Öberg et al. 2009c and Paardekooper et al. 2016b can be expected.

The mass peak at m/z = 33 is due to species with an elemental composition of NH_3O. The molecular ion of hydroxylamine (NH_2OH) could be a carrier of this signal, as is the case for protonated methanol or a fragment of hydrogen peroxide (H_2O_2). Contributions of the latter two are less likely, as mass signals at m/z = 32 (unfragmented methanol) and 34 (unfragmented hydrogen peroxide) are relatively low. In previous work, NH_2OH was shown to form through hydrogenation of NO (Fedoseev et al. 2012) and was recently detected in space (Rivilla et al. 2020).

In the case of peaks at m/z = 28-30, an increase is due to multiple species. The most likely contributors include carbon monoxide (CO)/N_2, formaldehyde (H_2CO), methanimine (CH_2NH) and fragments of bigger COMs. Specifically, primary amines have their characteristic, strong fragment at m/z = 30 (CH_2NH_2). For the water dominated experiments, the ratio of 29 to 30 is reversed upon longer photolysis, which may reflect a growing presence of a family of primary amines. All these assignments are also consistent for experiments with increased water content and (non)shifts observed for ^{18}O. Formation of imines and amines in the ice might proceed via excited radicals reacting with the CN bond of CH_3CN, for instance:

$$CH_3CN + 2H \rightarrow CH_3CHNH \tag{4.4}$$

$$CH_3CHNH + 2H \rightarrow CH_3CH_2NH_2 \tag{4.5}$$

Notes. Species previously detected using gas chromatography-mass spectrometry (GC-MS) after energetic processing of H_2O:CH_3CN ice are marked with an asterisk (*) based on Hudson et al. 2008

Table 4.3: Characteristic m/z peaks used for identification of photoproducts of the UV photolysis of the H_2O:CH_3CN (1:1 and 20:1) and $H_2{}^{18}O$:CH_3CN (20:1) ices.

	H_2O:CH_3CN m/z	$H_2{}^{18}O$:CH_3CN m/z	Elemental composition	Proposed molecular species	Name
$C_xH_yN_z$	2	2	H_2	H_2	mol. hydrogen
	16	16	CH_4	CH_4	methane*
	26, 27	26, 27	HCN	HCN/HNC	hydrogen (iso)cyanide *
	42, 43	42, 43	C_2H_5N	CH_3CHNH	imine (R−CHNH)
	44, 45	44, 45	C_2H_7N	$CH_3CH_2NH_2$	amine ($R-CH_2NH_2$)
	52	52	C_2N_2	CNNC/CNCN	cyanogen/isocyanogen
	26, 52, 53	26, 52, 53	C_3H_3N	CH_2CHCN	2-propenenitrile
	28, 54	28, 54	C_3H_5N	CH_3CH_2CN	propionitrile
	29, 55	29, 55	C_3H_5N	CH_3CH_2NC	ethyl isocyanide
	56	56	$C_2H_4N_2$	-	-
	66-69	66-69	$C_3H_xN_2$	-	-
	77-83	77-83	$C_4H_yN_2$	-	-
$C_xH_yO_z$	33, 34	37, 38	H_2O_2	H_2O_2	hydrogen peroxide
	28	30	CO	CO	carbon monoxide
	29, 30	31, 32	CH_2O	H_2CO	formaldehyde*
	31, 32	33, 34	CH_4O	CH_3OH	methanol
	44	48	CO_2	CO_2	carbon dioxide
	44, 29	46, 31	C_2H_4O	CH_3CHO	acetaldehyde *
	45, 46	47, 48	C_2H_6O	CH_3OCH_3	dimethyl ether
	45, 31	47, 33	C_2H_6O	CH_3CH_2OH	ethanol
	29, 46, 45	31, 50, 49	CHO_2	HCOOH	formic acid
	31, 60	33, 64	$C_2H_4O_2$	$HCOOCH_3$/$HOCH_2CHO$	methyl formate/glycolaldehyde
	43, 45, 60	45, 49, 64	$C_2H_4O_2$	CH_3COOH	acetic acid

-	H_2O:CH_3CN m/z	$H_2{}^{18}O$:CH_3CN m/z	Elemental composition	Proposed molecular species	Name
	31, 62	33, 66	$C_2H_6O_2$	$(CH_2OH)_2$	ethylene glycol
$C_xH_yN_zO_w$	33	35	NH_3O	NH_2OH	hydroxylamine
	43	45	CNOH	HNCO/HOCN/HCNO	(iso)cyanic acid/fulminic acid
	45	47	CH_3NO	NH_2CHO	formamide
	57	59	C_2H_3NO	$CH_3NCO/HOCH_2CN$	methyl isocyanate/glycolonitrile*
	58	60	C_2H_4NO	-	-
	59	61	C_2H_5NO	CH_3CONH_2/CH_3NHCHO	acetamide*/N-methyl formamide
	60	62	CH_4N_2O	NH_2CONH_2	urea
	62	64	C_2H_7NO	-	amine
	63	67	CH_5NO_2	-	-
	64	68	CH_5NO_2	-	-
other	19, 37, 55, 73	21, 41, 61, 81	$H_{2n+1}O_n$	$(H_2O)_nH^+$	water clusters H+
	60	-	C_2H_6NO	$(H_2O)(CH_3CN)H^+$	water/acetonitrile H+

From Fig. 4.8 it becomes clear that the higher mass range, m/z = 51-65, exhibits a picture of chemical complexity that is largely consistent with the lower mass range. Peaks at m/z = 51-57, associated with nitriles containing three C-atoms, are present in both the pure ice photolysis and in the 1:1 ice mixture. In the water dominated experiment (20:1), these are almost non detectable, most likely, due to an overabundance of water, which lowers the probability for CH_3CN molecules to stay next to each other in the ice.

New peaks, compared to the pure acetonitrile photolysis, appear at m/z = 58-60 and the peak at m/z = 57 is significantly more pronounced. Additionally, water dominated experiments give origin to new peaks at m/z = 61-64. Assigning elemental compositions to all peaks in this mass range (m/z = 51-65) is challenging due to low signals of the ^{18}O experiments, however, a few conclusions can be drawn. The peak at m/z = 57, for which a strong contribution from O-bearing species is visible, has an elemental composition of C_2H_3NO. There are several species consistent with this composition but the most likely candidates are glycolonitrile ($HOCH_2CN$) and methyl isocyanate (CH_3NCO). The first structure can be a direct result of a radical recombination (OH + CH_2CN) and the latter can be formed through an O-atom interacting with the triple bond of CH_3CN or its structural isotope, CH_3NC. The assignment of CH_3NCO is also supported by a recent study by Fourré et al. 2020, in which the relative thermodynamical stability of 40 isotopes of C_2H_3NO is compared. The clearly visible peak at m/z = 58 is associated with an elemental composition of C_2H_4NO, which is confirmed with a shift to m/z = 60. Considering the available molecular reservoir, the peak at m/z = 59 can be assigned to an elemental composition of C_2H_5NO. Newly formed species consistent with this observation include acetamide (CH_3CONH_2) and N-methyl formamide (CH_3NHCHO), with the first molecule being the most stable isomer (Lattelais et al. 2010). These may form in O/OH radical reactions involving CH_3CN and its structural isomer CH_3NC, followed by H-atom additions, but as the involved energetics are unknown, such a conclusion only can be treated with care.

Peak 60, which significantly increases for water dominated ices, can be explained by contributions from two stable combinations of elements: $C_2H_4O_2$ or CH_4N_2O. The peak shifts observed in the ^{18}O experiments, point to a major contribution from the species with one oxygen atom. One of the structures, that is potentially present is a molecule of astrobiological context, urea (NH_2CONH_2). This would be consistent with the Wohler synthesis. The previously demonstrated formation pathways of urea on interstellar grains analogues includes radical recombination of NH_2 and $CONH_2$ (Raunier et al. 2004; Ligterink et al. 2018a).

In water dominated experiments, additional peaks appear at m/z = 61-64. These peaks are shifted to 64-68 range in the ^{18}O experiments, indicating a presence of two oxygen atoms in the fragments. A possible corresponding elemental composition is CH_xNO_2, where x = 3-5.

The chemical complexity continues to increase as many peaks are seen in the higher m/z range. This indicates that upon VUV irradiation of CH_3CN (embedded in water) ices, even larger COMs with at least six or more C-, N- and/or O-atoms are formed. A specific assignment is not possible at this stage, but this observation on its own is interesting, as it shows that CH_3CN can act as an efficient precursor species in the formation of large N-containing COMs.

4.3.3 Abstraction reactions in the ice at 20 K

The most abundant product of the photolysis of pure CH_3CN ice is HCN. In order to compare the HCN yield between different experiments, it is helpful to convert the molecular yields to formation rates in molecules per absorbed photon. For this, average photon absorption cross sections in the range 120-165 nm are used, which for CH_3CN and H_2O are 7.5×10^{-18} photons cm^{-2} and 2.3×10^{-18} photons cm^{-2}. For mixed ices, the absorption cross section is derived as an average between the constituents, considering the ratio between them. The efficiency of HCN formation, per destroyed CH_3CN, per absorbed photon, is similar for all studied ices. On average, 1000 absorbed photons lead to the destruction of 230 CH_3CN molecules and the formation of 200 HCN molecules, almost 10 times the amount of CH_4.

The dominating yield of HCN motivates further investigation of its formation route. The radical recombination formation pathway of HCN requires photodissociation of two CH_3CN molecules (CN+H recombination). Additionally, if radical recombination is the dominant reaction mechanism, the CH_4 formation yield should be comparable (CH_3+H route). The calculated yields are not in line with a radical-radical recombination scenario, thus, other reaction types need to be considered.

One of the alternative formation routes is an abstraction reaction with the general formula: H-X+CN $\rightarrow$ X+HCN, where X can be CH_2CN, CH_3, etc. This reaction of CH_2CN and a CN radical resulting in formation of HCN is strongly exothermic (99 kJ/mole), while a similar reaction including a CH_3 radical, and resulting in CH_4 formation is barely exothermic (8 kJ/mole). The calculations of enthalpies are based on values from Active Thermochemical Tables available via Argonne National Laboratory (Ruscic et al. 2004). This helps to account for a major difference in production rates of HCN and CH_4. A theoretical study will be necessary to test which is the most efficient formation mechanism of HCN in the H_2O:CH_3CN ice. The reaction type discussed above, of an excited radical with a neutral species, has been recently demonstrated to be efficient also at low temperatures for gas phase CH_3OH+OH and CH_3CN+CN (Shannon et al. 2013; Sleiman et al. 2016). Hence, this type of reactions should be considered in gas-grain astrochemical models, which is already the case in recent work by Jin & Garrod 2020.

4.3.4 Role of water in ice chemistry

Water, as the most abundant constituent of interstellar ice, plays an important role in the solid state chemical networks. The effects of water molecules on the ice chemistry observed in this work are in agreement with previous studies (e.g. Öberg et al. 2010b). In particular, it is found that the formation of O-rich species is increased with the water content. In the water dominated experiment, $m/z = 44$ is assigned to species containing two O atoms, consistent with the observed shift to $m/z = 48$, for ^{18}O experiments. This peak, assigned to CO_2, is less intense in the mixture with 1:1 ratio, in comparison to the mixture with 20:1 ratio, and is not present in the pure CH_3CN ice photolysis. Other O-bearing species exhibit a similar behaviour, which follows the water abundance in the ice. Consequently, as CH_3CN molecules are more diluted in a water rich ice, the abundance of nitrile based photoproducts (e.g. CH_3CH_2CN) decreases proportionally.

H_2O ice provides an environment in which nitriles can efficiently transform into

imines and amines, upon UV-photolysis. Previous studies already reported on these findings. An isomerization of CH_3CN to an imine was demonstrated during UV photolysis by Hudson & Moore 2004, however, this was not studied in the water environment. In another study, Nguyen et al. 2019 performed an experimental and theoretical investigation of hydrogenation of CH_3CN. The study demonstrated a high energy barrier for hydrogenating the CN bond: between 0.06 - 0.22 eV, depending on the used level of theory. The analysis of the mass spectra in figure 4.6 shows evidence for effective hydrogenation of the CN bond, which leads to formation of imines and amines, in a water rich ice. This must be due to the energetic radicals produced in photodissociation of the water molecules. Indeed, the average translation energy carried by an H radical following water dissociation is between 1.5 - 2.5 eV (Andersson & van Dishoeck 2008), larger than the calculated barrier of 0.22 eV. Following the first hydrogenation of the CN bond, subsequent H atom additions have a lower energetical barrier, which eventually leads to a formation of imines and amines.

The chemical complexity observed in the photolyzed mixed ices goes beyond amines, specifically the formation of amides (molecules containing the $-C(=O)NH_2$ functional group) is observed. During the photolysis of the mixed ices, the mass peaks associated with amides (m/z = 57-59) appear after 2 min of irradiation (see Fig. 4.8), hence a formation pathway involving many steps is unlikely. Here, formation of amides is suggested via O-/OH-radical interacting with the triple bond of CH_3CN. Photodissociation of H_2O using photons in an energy range between 8.5-10.5 eV leads to an electronically excited $OH(A^2)$ and $O(^1D)$ (van Harrevelt & van Hemert 2008), which can interact with the CN bond to form amides. This chemical route, however, requires further verification. At least two other pathways to form amides are known. Both might be more relevant towards the end of our experiments, as multiple chemical steps are involved. One pathway is demonstrated by Ligterink et al. 2018a, where formation of CH_3CONH_2 proceeds via recombination of the NH_2CO radical (formed from NH_2+CO) with a CH_3 radical. An alternative route is through breaking of the C-OH bond in any carboxylic acid (e.g. acetic acid, CH_3COOH) and attaching a -NH, NH_2 or -NRH (from ammonia or any amine) to the leftover C=O structure will yield formamide (NH_2CHO).

4.4 Astrophysical implications and conclusions

N-bearing COMs are commonly observed towards diverse environments, yet the chemical network leading to their formation is still unclear. An observational study focused on the origin of N-bearing COMs in the Galactic Center quiescent giant molecular cloud, G+0.693, by Zeng et al. 2018 concluded that species such as CH_3CN, HC_5N, HNCO, and NH_2CHO are transferred to the gas phase from dust grains. The gas phase abundances of CH_3CN observed in protoplanetary disks, photodissociation regions (PDR) and dark, dense molecular cores, also imply that CH_3CN is released from icy mantles (Loomis et al. 2018; Gratier et al. 2013). These findings are in agreement with the laboratory work presented here that shows that upon vacuum UV irradiation of H_2O:CH_3CN ice a large amount of N-bearing COMs can be formed. This is not fully unexpected, as the molecular structure of acetonitrile (CH_3-CN) resembles that of methanol (CH_3-OH) that has been shown to be an important parent molecule to O-bearing COMs. Actually, as methanol is found to be formed upon UV photolysis of

H_2O:CH_3CN ice, the experiments analyzed here also offer pathways towards O-(and N/O-)bearing COMs. It should be noted, though, that methanol is more abundant than CH_3CN; also other nitrogen precursors, such as NO and NH_x radicals may play a role in the formation of N-bearing COMs (see for example Congiu et al. 2012, Muñoz Caro et al. 2014, Jones et al. 2011 and Ioppolo et al. 2021). To fully benefit from the work presented here, modeling will be needed to place the importance of CH_3CN ice chemistry in the larger astrochemical context. For this it also will be important to better understand how CH_3CN forms.

It should also be noted that pure CH_3CN ice does not exist in space, but for the purpose of this study a diluted H_2O:CH_3CN (20:1) mixture simulates the potential role acetonitrile can play. In fact, the involvement of the methyl radical, CH_3, in CH_3CN formation would position its formation stage in the water rich phase (see Öberg et al. 2008; Qasim et al. 2020). There are different astronomical environments where the processes described here may be at play. In dense dark clouds, it is generally assumed that solid state astrochemical processes are driven by atom addition reactions (Linnartz et al. 2015). It is here that smaller molecules like H_2O, NH_3 and HNCO or CH_4 form, as well as larger species including glycerol (Fedoseev et al. 2017). UV induced chemistry is considered to be less important (Chuang et al. 2017), but cannot be excluded. In dark clouds ices are exposed to cosmic ray induced UV irradiation. In the more translucent cloud areas, as well as in protoplanetary disks, UV induced chemistry takes over. During the star formation cycle, these energetically processed ices are eventually desorbed, allowing for the detection of COMs in the gas phase. Hence, it is interesting to compare the products detected during the UV photolysis of the CH_3CN and H_2O:CH_3CN (20:1) ices with astrochemical observations and models.

After an exposure of a pure CH_3CN ice to a photon fluence of 8.9×10^{17} photons cm^{-2}, 25% of CH_3CN molecules are converted to other species. The products which are larger than the parent species, supplying the N-bearing COM reservoir, make up for 25% of the lost parent molecules. The same analysis was performed for the water dominated mixture (20:1). 25% of water molecules were depleted while 85% of acetonitrile molecules were consumed. This demonstrates that water effectively prevents the recombination of CH_3CN and enhances its photoconversion by providing reactive O, OH, and H radicals. Thus, on the dark cloud time scales, a high conversion rate of CH_3CN into the photoproducts can be expected.

The photolysis of pure CH_3CN ice leads to isomerization or formation of other nitrile based species. HCN is the most abundant product of photolysis, but many other species are formed including: CH_3CH_2CN and $NCCH_2CH_2CN$. The types of reactions leading to this complexity are radical-radical recombinations (e.g. CH_3+$CH_2CN \rightarrow CH_3CH_2CN$), radical-molecule interactions (e.g. CH_3CN+$CN \rightarrow HCN$+CH_2CN) and (de)hydrogenation reactions (e.g. CH_3CH_2CN - 2H $\rightarrow CH_2CHCN$ and CH_3CN + 2H $\rightarrow CH_3CHNH$). Specifically for HCN, it is demonstrated that radical-radical interactions alone are not sufficient to account for its formation yield.

The chemical complexity resulting from the pure CH_3CN photolysis is shown in the upper part of Figure 4.9. All photoproducts, except for NCCN and $NCCH_2CH_2CN$, have been observed in the ISM. However, the presence of NCCN in the ISM is implied by detections of two closely related species: a metastable isomer CNCN and the protonated form of cyanogen, $NCCNH^+$ (Agúndez et al. 2015, 2018). Both of the species are detected in dense clouds L483 and TMC-1. The known formation mechanism of NCCN includes an exothermic gas phase pathway via neutral-neutral

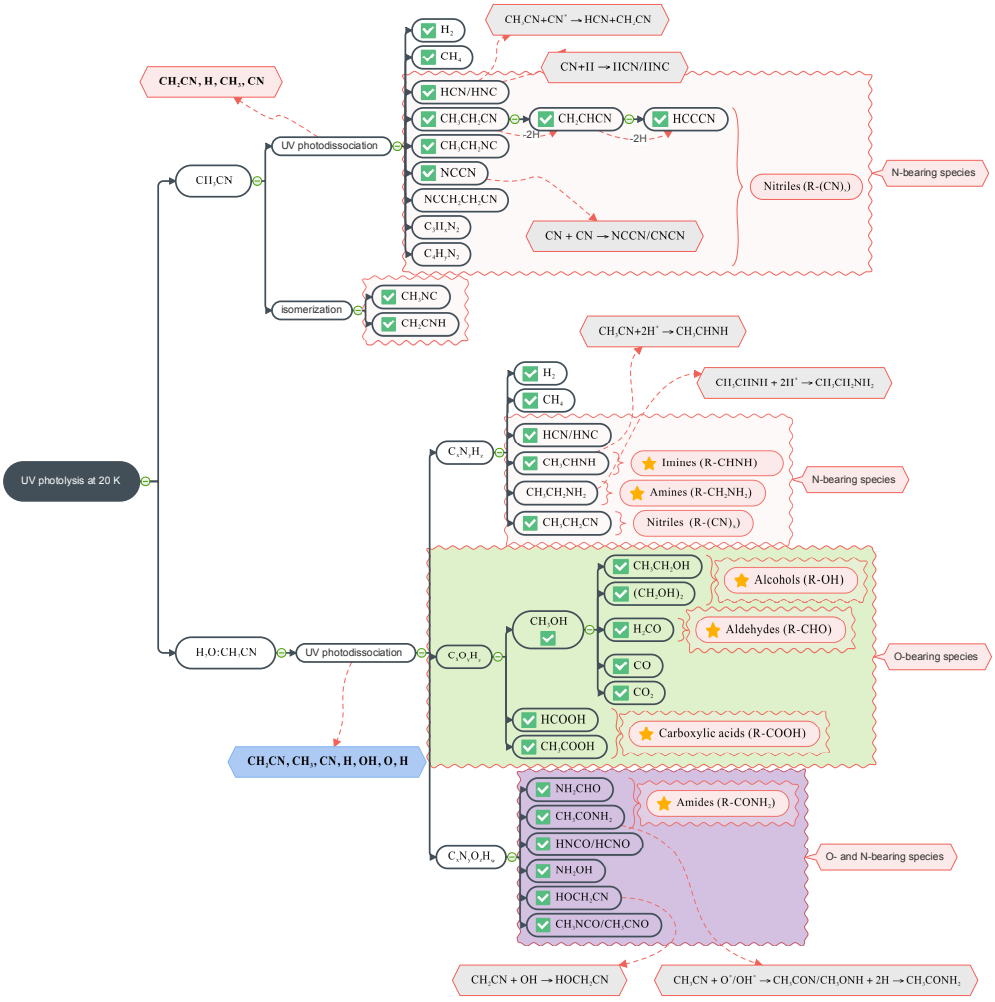

Figure 4.9: An overview of products of UV photolysis of CH_3CN and H_2O:CH_3CN (20:1) ices at 20 K. Groups of molecules uniquely produced in the ice mixtures are marked by a yellow star. The species marked with a check mark have been detected in the ISM. NCCN is marked as detected due to observations of other species which are chemically related and imply its presence in the ISM (Agúndez et al. 2015).

reaction: CN+HCN → NCCN+H (Petrie et al. 2003). Alternatively, it is suggested that it might be also formed on dust grains through recombination of two CN radicals. This is indeed the case in our experiments. It is important to note, that the formation of NCCN/CNCN, as well as $NCCH_2CH_2CN$, is only visible for the pure CH_3CN ice photolysis, thus both species could be used as tracers of an ice that is rich in CN.

In a more realistic case, the CH_3CN is diluted in a H_2O ice, and this mixture yields significantly more complexity (shown in the lower part of Fig. 4.9). Even though it is not possible to assign all observed mass peaks unambiguously to specific carrier molecules, the mass spectra reveal trends that can be connected to chemical families. It is clear that a diverse number of larger N-containing COMs is formed upon UV irradiation of H_2O:CH_3CN ice. In the presence of water, the CN bond of acetonitrile can be hydrogenated, leading to the formation of imines and amines. In the study by Loomis et al. 2013, CH_3CHNH was observed towards Sgr B2(N) and now its formation pathway is demonstrated to be possible via hydrogenation of CH_3CN. The hydrogenation process continues until $CH_3CH_2NH_2$ is formed, which has the highest abundance towards the end of the UV photolysis. However, this molecule is yet to be detected in the ISM.

The reactivity of O and OH radicals with the CN bond provides a chemical link between the O- and N-bearing chemical networks. Specifically, formation of amides is suggested to proceed via the O/OH radical interacting with the parent nitrile molecule, which, when followed by hydrogenation reaction, yields CH_3CONH_2. Other formed N- and O-bearing species include HNCO/HCNO, NH_2OH, CH_3NCO and $HOCH_2CN$. All of these molecules, except for an CH_3NCO isomer, namely, CH_3CNO, have been observed in the ISM. The formation mechanism of $HOCH_2CN$, observed in IRAS-16293B (Zeng et al. 2019) and in Serpens SMM1-a (Ligterink et al. submitted), is suggested to have a solid state route. In our experiments it most likely proceeds via OH + CH_2CN → $HOCH_2CN$, as both of these radicals are immediately available to react. Alternatively, this product might be formed through reactions of NH_3 with H_2CO and $NH_4^+OCN^-$ (Danger et al. 2012).

To conclude, the UV photolysis of pure CH_3CN ice yields larger nitriles including NCCN/CNCN, CH_3CH_2CN and $NCCH_2CH_2CN$. In addition, it is demonstrated that H atom abstraction reactions are an efficient formation pathway of HCN. The UV photolysis of an astronomically relevant H_2O:CH_3CN ice at 20 K, leads to formation of larger (at least up to 6-7 C/N/O-containing) molecules with the functional groups of: imines, amines, amides, large nitriles, carboxylic acids and alcohols. Photodissociation products of H_2O play a key role in this chemical network. Hydrogenation of the CN bond leads to formation of imines and amines, whereas the interaction of O- and OH with the CN bond results in formation of amides. The identification of photoproducts (see Fig. 4.9), provides a tool to link astronomical observations of (N- and O-bearing) COMs to the underlying solid state processes in which these are formed. In this study it is shown that CH_3CN can play a central role in the chemical network that ultimately results in a further increase of molecular complexity in space. Many of these species already have been identified in recent studies (van Gelder et al. 2020b, Ligterink et al. 2020, submitted and Nazarri et al. 2020, in preparation) other species not identified yet, may be well present in the ISM, following the work presented here.